[Note: This is a preprint of a document submitted for publication. Contents of this document should not be quoted or referred to without permission of the author(s).]

To be published in *Proceedings of Multinational Congress on Electron Microscopy*
Parma, Italy, September 13–17, 1993

# PROBING INTERFACE STRUCTURE AND BONDING AT ATOMIC RESOLUTION BY STEM

S. J. Pennycook, N. D. Browning, D. E. Jesson, and M. F. Chisholm

Solid State Division
Oak Ridge National Laboratory
Oak Ridge, Tennessee 37831



SOLID STATE DIVISION
OAK RIDGE NATIONAL LABORATORY
Managed by
MARTIN MARIETTA ENERGY SYSTEMS, INC.
under
Contract No. DE-AC05-84OR21400
with the
U.S. DEPARTMENT OF ENERGY
Oak Ridge, Tennessee 37831-6030

June 1993

# PROBING INTERFACE STRUCTURE AND BONDING AT ATOMIC RESOLUTION BY STEM

S. J. Pennycook, N. D. Browning, D. E. Jesson, and M. F. Chisholm
Solid State Division, Oak Ridge National Laboratory, Oak Ridge, Tennessee 37831-6030

## 1. ATOMIC RESOLUTION IMAGING AND ANALYSIS

Figure 1 shows schematically how an atomic-resolution Z-contrast image may be formed in a high-resolution scanning transmission electron microscope (STEM). A crystal, oriented to a low-order zone axis, is scanned by a coherent probe focused to a diameter less than the spacing between the columns. We form a high-resolution image based on close-encounter scattering events, using the high-angle annular detector proposed by Howie (1979). This breaks the coherence of the imaging process (Jesson and Pennycook 1993), and we can consider each atom to scatter independently with a cross section that approaches a $Z^2$ dependence on atomic number. A Bloch wave analysis shows how the resolution is determined by the incident probe intensity profile (Pennycook and Jesson 1991, 1992) thus providing enhanced resolution over coherent phase contrast imaging. In a perfect crystal, dynamical diffraction manifests itself as a thickness-dependent columnar channeling effect (including absorption) which simply scales the scattering cross section. Note, however, that differences in high angle scattering due to channeling effects are always less than differences due to composition, so that we retain the most important feature of incoherent imaging, its intuitive interpretability. In imperfect crystals of course, $s \rightarrow p$ and $p \rightarrow s$ Bloch state transitions result in depth dependent contrast effects (Cowley and Huang 1992, Perovic 1992).

The key advantage for materials applications is that no model structures are required to interpret the images to first order, so that unexpected interfacial phenomena will be immediately apparent. For example, the Z-contrast image in Fig. 2. was taken with a VG Microscopes HB501UX STEM operating at 100kV with a probe size (FWHM imtensity) of 2.2Å. It shows clear compositional ordering at a $CoSi_2$/Si(100) interface made by high-dose Co implantation and annealing (Chisholm et al. 1993). It is apparent from the image that the ordering must involve Co atoms, whereas all models considered in previous phase contrast studies have considered only Si ordering. The Co ordered structure does however produce simulated phase contrast images in good agreement with published results.

In direct analogy with this description of column-by-column imaging, close-encounter *inelastic* scattering events may be used as the basis for atomic-resolution microanalysis. In fact, since both signals may be detected simultaneously (see Fig. 1), the Z-contrast image may be used to position the probe on selected individual atomic columns for microanalysis. Modern CCD-based parallel EELS systems provide optimum detection efficiency (Browning and Pennycook 1993), and Fig. 2 shows raw spectra and the resulting Co profile across the $CoSi_2$/Si(100) interface. Each spectrum was obtained by centering a line scan over each plane in turn using the Z-contrast signal displayed on an oscilloscope, then acquiring a Co-L edge for 5s [Browning et al. 1993 (a)]. The EELS result clearly demonstrates atomic resolution, the same as seen in the Z-contrast image itself. To ensure incoherent, close-encounter events, we again use a large (30 mrad) collection semiangle which averages over dynamical effects on the outgoing inelastically scattered electrons and also improves the localization of the energy transfer.

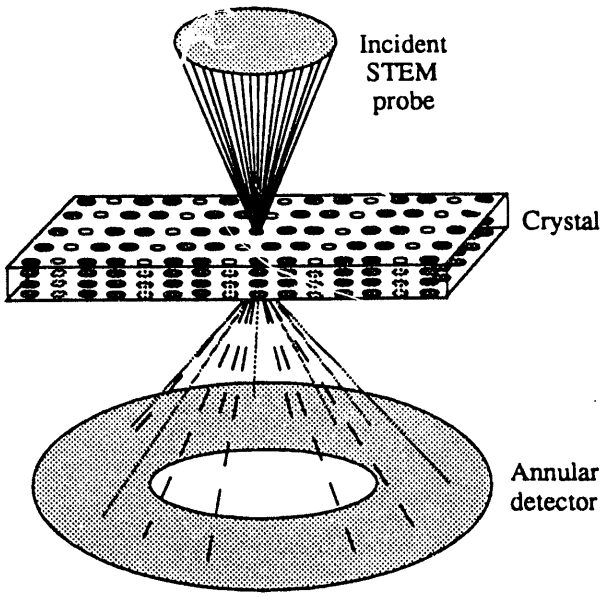


Fig. 1. The formation of a Z-contrast image in a STEM through the use of a Howie detector (typical inner semiangle 75 mrad).

Fig. 2. (a) EEL spectra obtained from individual atomic planes using the Z-contrast image (b) to locate the probe. The Co profile (c) exhibits the same spatial resolution as the image, consistent with the theoretical probe profile.

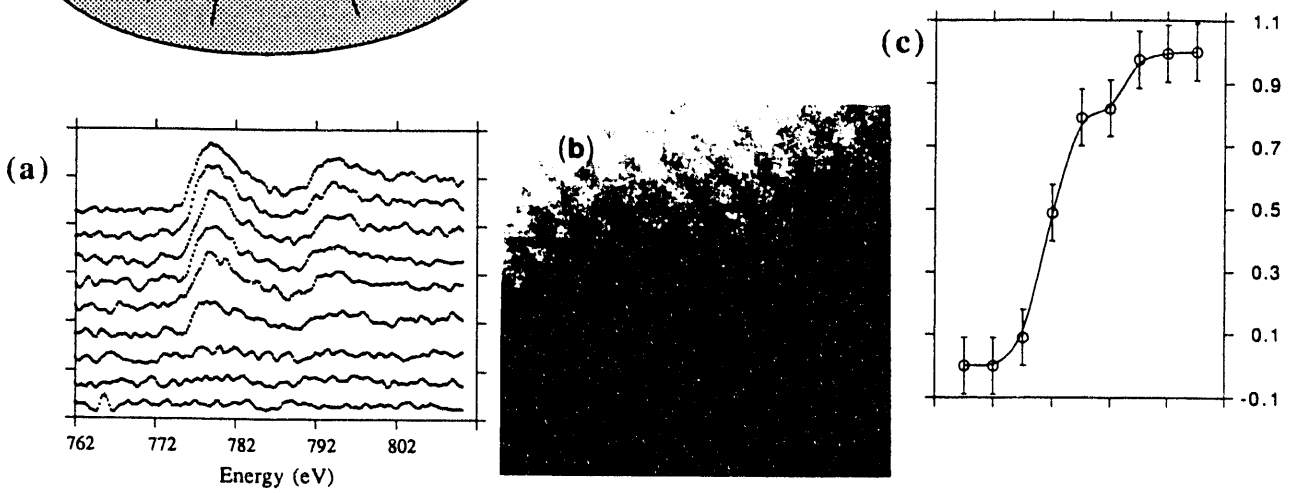


## 2. INSIGHTS INTO THE GROWTH AND RELAXATION OF STRAINED LAYERS

It is well known that the surface morphology of a strained epitaxial layer is unstable (Srolovitz 1989), although little is known concerning the time evolution under the highly nonequilibrium conditions of low-temperature growth. By depositing 2 monolayer Ge marker layers during the growth of $Si_{.5}Ge_{.5}$ alloy layer, the cross section image in Fig. 3 provides a direct view of the evolving surface morphology. It can be seen that the growing surface remains relatively flat up to a thickness of about 25 nm, almost an order of magnitude greater than the equilibrium critical thickness. Most surprising, however, is the evolution of sharp, cusp-like features at about 40 nm, which persist for 20 nm or so before the surface again flattens out. The development of the cusp can be well modeled on the basis of the usual contributions from local surface curvature and elastic energy to the surface chemical potential as shown in Fig. 3 (Jesson et al. 1993). The high energy associated with the sharp cusp is more than offset by the release of elastic energy within the rest of the island. In fact, the simulations indicate that a runaway situation can develop whereby coherent islands will be formed. In our case, another process has occurred to relieve the strain, the nucleation of a misfit dislocation. Modeling the dislocation nucleation in the usual way, but in the nonuniform field of the cusp (treated as a classical crack), we find that nucleation of a 60° dislocation is effectively barrierless even using a high core energy parameter $\alpha = 4$. The corresponding nucleation at a flat surface, however, encounters a 70 eV activation barrier (see Fig. 4).

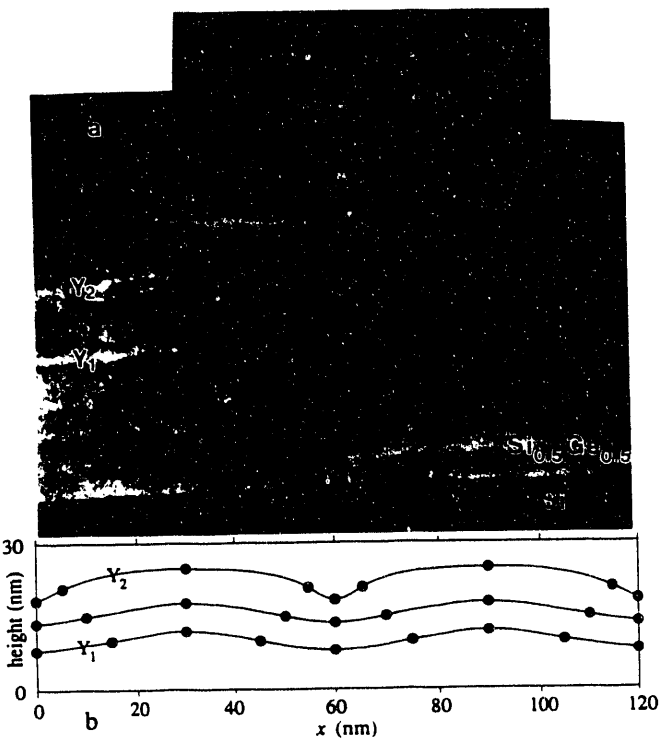


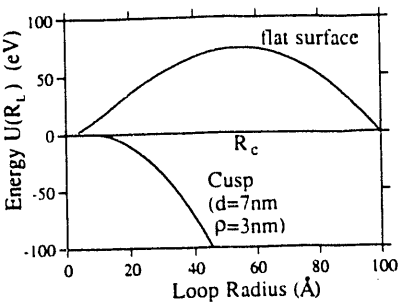


Fig. 4. Total energy for nucleation of a 60° dislocation in $Si_{.5}Ge_{.5}$ at a flat surface and in the stress concentration of the cusp, assuming a dislocation core parameter of 4.

Fig. 3.(a) Z-contrast image showing development of a sharp cusp during growth of a $Si_{.5}Ge_{.5}$ strained epitaxial layer.
(b) Simulated cusp development based on evaluation of the surface chemical potential at the peak, valley, and point of inflexion.

## 3. MAPPING SUPERCONDUCTING PROPERTIES ON THE SCALE OF THE COHERENCE LENGTH

Measurement of local hole concentration in $YBa_2Cu_3O_{7-\delta}$ can be obtained from the pre-edge feature on the O-K absorption edge to an accuracy of approximately 5% (Browning et. al. 1992). These measurements may be achieved on a scale below the coherence length, in principle with the same resolution as the image itself, the atomic scale. Equally important, a time sequence may be taken to test for beam damage or oxygen loss in the specimen during analysis. If no such effects are seen, the spectra may be added to improve statistics. Figure 5 shows hole concentration profiles across two grain boundaries in a polycrystalline film of YBCO on a YSZ substrate [Browning et. al. 1993 (b)]. The asymmetric boundary shows a deep cusp in hole concentration that extends over 50Å either side of the boundary. This is much further than the range of structural disorder observed in the Z-contrast image. In contrast, the symmetric boundary shows no evidence of any hole depletion and no evidence of structural disorder in the image. We believe this observation provides the first microscopic evidence that not all high angle grain boundaries act as weak links.

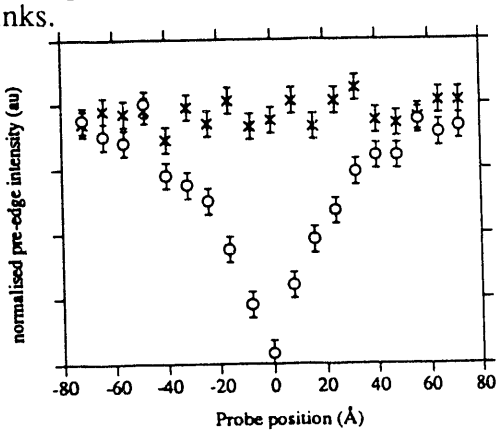


Fig. 5. Hole concentration profiles across symmetric (crosses) and asymmetric (circles) grain boundaries, obtained by analyzing the pre-edge feature of the oxygen K loss. EELS spectra were recorded every 8 Å with 10 seconds total acquisition time per spectrum. Note the sensitivity and spatial resolution obtained at the cusp, and the lack of hole depletion at the symmetric boundary.

## 4. FUTURE DIRECTIONS

Combining atomic-resolution imaging and analysis on a single microscope appears to be a very powerful method of characterizing the structure, composition, and electronic properties of interfaces without the need for any prior knowledge or model structures. Invariably, this reveals new insights into materials and their growth phenomena. Increasing the accelerating voltage from the current 100 kV to 300 kV has recently demonstrated a reduction in probe size to 1.4 Å through the resolution of the Si dumbbell (Fig. 6). In the future, we can also expect to see more use of image reconstruction, through maximum entropy methods for example (Fig. 7). Reconstruction is particularly robust for incoherent imaging since there are no oscillations of the transfer function to deal with.

Fig. 6. Resolution of the dumbbells in Si⟨110⟩, spacing 1.36 Å, using a 300 kV STEM with a 1 mm $C_S$ objective lens.

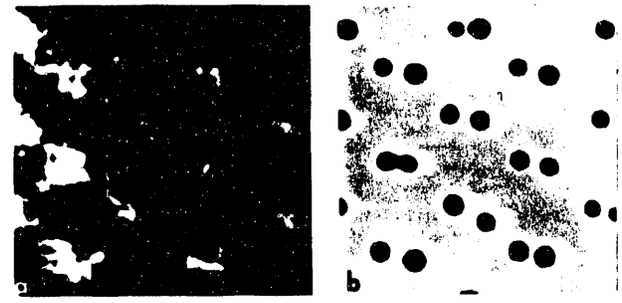

Fig. 7. (a) 100 kV STEM image of the Si⟨110⟩ dumbbells with 2.2 Å resolution. (b) Maximum entropy reconstruction using the Cambridge MemSys5 software of Gull and Skilling (1984).


## 4. ACKNOWLEDGMENT

This research was sponsored by the Division of Materials Sciences, U.S. Department of Energy, under contract DE-AC05-84OR21400 with Martin Marietta Energy Systems, Inc.


## 5. REFERENCES


Browning, N. D., Yuan, J. and Brown, L. M. 1992 Physica C 202 12.

Browning, N. D. and Pennycook, S. J. 1993 Microbeam Analysis 2 81.

Browning, N. D., McGibbon, M. M, Chisholm, M. F., and Pennycook, S. J. in press 1993 (a) Proc. Microscopy Society of America (San Francisco Press).

Browning, N. D., et. al. submitted 1993 (b) Physica C.

Chisholm, M. F., Jesson, D. E., Pennycook, S. J., and Mantl S. in press 1993 Proc. Microscopy Society of America (San Francisco Press).

Chisholm, M. F., Pennycook, S. J., and Jesson, D. E. 1990 MRS Symp. Ser. No. 139 447.

Cowley, J. M. and Huang, Y. 1992 Ultramicroscopy 40 171.

Gull, S. F. and Skilling J. 1984 IEE Proc. 131F 646.

Howie, A. 1979 J. Microsc. 117 11.

Jesson, D. E. and Pennycook S. J. in press 1993 Proc. Microscopy Society of America (San Francisco Press).

Jesson, D. E., et. al. submitted 1993 Physical Review Letters.

Pennycook, S. J. and Jesson, D. E. 1991 Ultramicroscopy 37 14.

Pennycook, S. J. and Jesson, D. E. 1992 Acta Metall. Mater. 40 Suppl. S149.

Perovic, D. D. 1992 Proc. Electron Microscopy Society of America (San Francisco Press) p. 1336.

Srolovitz D. J. 1989 Acta. Met. 37 621.

# END

# DATE FILMED

11/16/93